

High speed atomic force microscopy enabled by a sample profile estimator

Peng Huang and Sean B. Andersson

Citation: *Appl. Phys. Lett.* **102**, 213118 (2013); doi: 10.1063/1.4808211

View online: <http://dx.doi.org/10.1063/1.4808211>

View Table of Contents: <http://apl.aip.org/resource/1/APPLAB/v102/i21>

Published by the [American Institute of Physics](http://www.aip.org).

Additional information on *Appl. Phys. Lett.*

Journal Homepage: <http://apl.aip.org/>

Journal Information: http://apl.aip.org/about/about_the_journal

Top downloads: http://apl.aip.org/features/most_downloaded

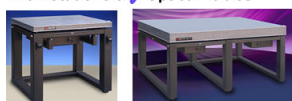
Information for Authors: <http://apl.aip.org/authors>

ADVERTISEMENT



Improve your Images with Minus K's
Negative-Stiffness Vibration Isolation

Workstations & Optical Tables



Custom Applications



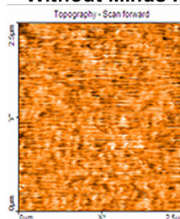
Bench Top Isolators



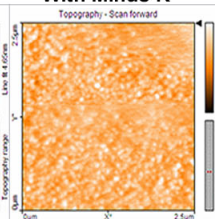
Multi Isolator Systems



Without Minus K



With Minus K



Floor Platforms



High speed atomic force microscopy enabled by a sample profile estimator

Peng Huang¹ and Sean B. Andersson^{1,2,a)}

¹Department of Mechanical Engineering, Boston University, Boston, Massachusetts 02215, USA

²Division of Systems Engineering, Boston University, Boston, Massachusetts 02215, USA

(Received 18 March 2013; accepted 16 May 2013; published online 31 May 2013)

In this paper, an estimation scheme for imaging in Atomic Force Microscopy (AFM) is presented which yields imaging rates well beyond the bandwidth of the vertical positioner and allows for high-speed AFM on a typical commercial instrument. The estimator can be applied to existing instruments with little to no hardware modification other than that needed to sample the cantilever signal. Experiments on a calibration sample as well as lambda DNA are performed to illustrate the effectiveness of this method. These show a greater than an order-of-magnitude improvement in the imaging rate. © 2013 AIP Publishing LLC. [<http://dx.doi.org/10.1063/1.4808211>]

In atomic force microscopy (AFM),¹ a controller is used to tightly regulate the tip-sample interaction. Topological information is typically derived from the corresponding motion of the vertical (z) actuator.² As a result, the rate of taking a single measurement is limited by the bandwidth of the z -piezo loop and a high overall frame rate comes at a cost in terms of the scanning size and the resolution.³ Advanced hardware and specialized controller designs have been developed and integrated in a variety of commercial and research AFMs^{4–6} to create high-speed AFM (HS-AFM) instruments that approach video-rate imaging.

Algorithmic approaches to HS-AFM seek to work with existing hardware and improve imaging rates by alternative approaches to selecting and acquiring measurements or through signal processing techniques to extract more information from poor signals. Because they require little to no hardware modification, they can be applied to existing AFMs to improve imaging rates as well as to HS-AFM instruments for even further gains. One example is our previous work for high-speed imaging of biopolymers and other string-like samples.⁷ In this local raster scan, imaging time is reduced by using feedback to focus the measurements in the region of interest, namely, close to the biopolymer. Its effectiveness is due in part to the structure of the sample, and the approach is therefore limited to string-like samples. To allow for more general samples, in this work we present a fast estimation scheme that determines the sample profile at rates independent of the z -actuator loop. As a result, high-speed imaging can be achieved by integrating this signal with the conventional raster motion executed by any commercial AFM. It is also compatible with novel scanning trajectories, such as spiral scanning,⁸ cycloids,⁹ Lissajous figures,¹⁰ and our local raster scan.⁷ Driven by the requirements of imaging soft samples, we focus on intermittent (tapping) mode AFM.

There are a few existing estimation-based approaches to AFM imaging. One relies on building an advanced controller based on robust control theory for the z -piezo.¹¹ By taking advantage of the structure of the controller, a signal was derived with a transfer function of 1 to the sample profile, implying an infinite bandwidth in the estimator. It is, however, only applicable to a particular instrument and relies on

the specific controller. Given the fact that most commercial AFMs are equipped with a PI controller,² this method requires significant modification to the operation of the instrument.

Our approach is perhaps most closely related to transient-mode AFM (TM-AFM).¹² Based on signal processing techniques, TM-AFM does not require hardware modifications to the AFM other than possibly access to the unfiltered cantilever signal. This method uses an observer of the cantilever dynamics together with the assumption that at high scan rates, the transition of the tip from substrate to sample can be approximated as an abrupt input to the cantilever system. As a result, the rising edges of the sample are able to be detected by the mismatch of the initial condition between the system output and the observer estimate. While offering high-speed edge detection, it does not produce a sample profile estimate.

Inspired by TM-AFM, our method begins with an observer of the cantilever and then builds an estimator of the sample profile under the assumption that the AFM is operated at a sufficiently high-speed.¹³ The bandwidth of the sample profile estimator is not limited by the z -piezo loop (typically on the order of single to the low tens of kHz²) but rather by the resonance of the cantilever (typically on the order of tens of kHz to MHz) and by the lateral scanning speed. The overall imaging rate can be improved at least an order of magnitude depending upon the probes used as well as the x - y stages.

To develop the estimator, the cantilever system in tapping mode is modeled as a damped spring system driven to oscillate near its resonance. As a result, the cantilever system can be written as

$$\ddot{y}(t) + a_2\dot{y}(t) + a_1y(t) = b_1(u(t) + n_1(t)) + b_2u_2(t) + n_T(t), \quad (1)$$

where a_1 and a_2 are system coefficients that can be computed by the resonance and the quality factor of the cantilever, $u(t)$ is the sinusoidal driving input, $n_1(t)$ is the input noise, $u_2(t)$ is the input due to the sample surface change, and $n_T(t)$ is the thermal noise. Define

$$w_1(t) = b_1n_1(t) + n_T(t), \quad w_2(t) = b_2u_2(t).$$

^{a)}Electronic mail: sanderss@bu.edu.

With this, Eq. (1) can be expressed in the state space form in discrete-time as

$$x(k+1) = Fx(k) + Gu(k) + w_1(k) + w_2(k), \quad (2a)$$

$$y(k) = Hx(k) + v(k), \quad (2b)$$

where F , G , and H are the state matrix, the input matrix, and the output matrix, respectively, in discrete time, $E[w_1(k)] = 0$, $E[w_1(k)w_1^T(k)] = Q_1$, $v(k)$ is the measurement noise with $E[v(k)] = 0$ and $E[v(k)v^T(k)] = R$, and $w_2(k)$ is due to the change in the sample profile. This last term is viewed as deterministic but unknown. Note that the noise parameters Q_1 and R can be experimentally measured. A Kalman filter for Eq. (2) is given by

$$\hat{x}(k|k-1) = F\hat{x}(k-1|k-1) + Gu(k-1), \quad (3a)$$

$$\hat{x}(k|k) = \hat{x}(k|k-1) + K\gamma(k), \quad (3b)$$

where K is the steady-state Kalman observer gain and $\gamma(k) = y(k) - H\hat{x}(k|k-1)$ is the measurement residual, also known as the innovation process.

As the cantilever is scanned over the sample surface, the changes in the sample profile enter the model through the (unknown) input w_2 . Since the filter Eq. (3) does not account for this term, the innovation process contains the information about this disturbance. This concept was first introduced in Ref. 12, where the rising edge of $w_2(k)$ was modeled as an abrupt input to the system under the condition that the AFM is operated at high speed. The method was shown to be effective in detecting the rising edges of a sample with a bandwidth approximately one-fourth of the resonance of the cantilever.¹¹

To extract information beyond sample edges from w_2 , we develop its relationship to the sample profile. Consider, then the Kalman filter in Eq. (3). Through some manipulation the measurement residual can be shown to be

$$\begin{aligned} \gamma(k) &= HF(x(k-1) - \hat{x}(k-1|k-1)) \\ &+ w_1(k-1) + w_2(k-1) + v(k). \end{aligned} \quad (4)$$

Taking the second-order expectation of both sides of Eq. (4) yields

$$E[\gamma(k)\gamma^T(k)] = HFP(k-1)F^TH^T + Q_1 + w_2^2(k) + R. \quad (5)$$

Here, $P(k-1)$ is the covariance of the estimate of the state. The value of $E[\gamma(k)\gamma^T(k)]$ can be estimated using the Mean Square Error (MSE) over a finite window with a size M as follows:

$$\widehat{\text{var}}[\gamma(k)] = \sum_{k-M+1}^k \frac{\gamma^2(i)}{(M-1)}.$$

The next step is to replace the covariance matrix P in Eq. (5) in terms of the second-order statistic of $\gamma(k)$. To do this, a straightforward derivation leads to

$$KH[x(k) - \hat{x}(k|k)] = (I - KH)K\gamma(k).$$

Taking the second expectation of both sides of this expression then yields $P(k-1)$ in terms of $\widehat{\text{var}}[\gamma(k)]$.

Using these results to invert Eq. (5) leads to an estimate of w_2 given by

$$\hat{w}_2(k) = (\widehat{\text{var}}[\gamma(k)] - f_{11}^2(1 - k_{11})^2\widehat{\text{var}}[\gamma(k-1)] - Q_1 - R)^{\frac{1}{2}}, \quad (6)$$

where we have used the fact that $H = [1 \ 0]^T$ and expressed the system and steady-state Kalman gain matrices as

$$F = \begin{pmatrix} f_{11} & f_{12} \\ f_{21} & f_{22} \end{pmatrix}, \quad K = \begin{pmatrix} k_{11} \\ k_{21} \end{pmatrix}.$$

The entries of F are determined by the (experimentally determined) parameters of the cantilever and those of K by the parameters and the noise matrices Q_1 and R .

As discussed above, $w_2(k)$ is the unknown disturbance driven by the tip-sample interaction due to the surface changes. The goal of the z -piezo controller is to compensate for this disturbance. As a result, the information content in $w_2(k)$ depends in part on the scanning speed. Let ω_B denote the bandwidth of the z -piezo controller. The signal $w_2(k)$ can be written (approximately) as

$$w_2(k) = h(s(k)) - \Gamma_{\omega_B}[r(k) - \mathcal{D}(y(k))], \quad (7)$$

where $s(k)$ is arclength, $h(\cdot)$ is the function capturing the tip-sample interaction due to changes in the sample profile and the vertical position of the cantilever, $r(k)$ is the reference input, $\mathcal{D}(\cdot)$ is the demodulation operator that determines the cantilever oscillation amplitude from the measurement y , and $\Gamma_{\omega_B}[\cdot]$ is an operator capturing the z -piezo motion with a bandwidth of ω_B .

If the scanning speed is slow enough such that the rate of individual measurements is well below ω_B , then the actuator closely tracks the changes in the surface. In this case, $w_2(k)$ is the tracking error. At slow speeds, then $E[\hat{w}_2(\infty)] = 0$ and

$$\widehat{\text{var}}[\gamma(\infty)] = \frac{Q_1 + R}{1 - f_{11}^2(1 - k_{11})^2} \triangleq \bar{V}.$$

At low scan speeds (relative to ω_B), the Kalman filter is essentially in steady state, leading to

$$\widehat{\text{var}}[\gamma(k)] \simeq \widehat{\text{var}}[\gamma(k-1)].$$

Using these results in Eq. (6) yields

$$\hat{w}_2(k) \simeq \sqrt{(1 - f_{11}^2(1 - k_{11})^2)(\widehat{\text{var}}[\gamma(k)] - \bar{V})}. \quad (8)$$

Since at low scan speeds, $\widehat{\text{var}}[\gamma(k)] \sim \bar{V}$, Eq. (8) implies that \hat{w}_2 is close to zero and contains very little useful information. As expected, then, at low speeds, sample profile estimation should be done using standard techniques based on the actuator output.

Consider now moderate scanning speeds close to (but less than) the bandwidth ω_B . As at slow speeds, $w_2(k)$

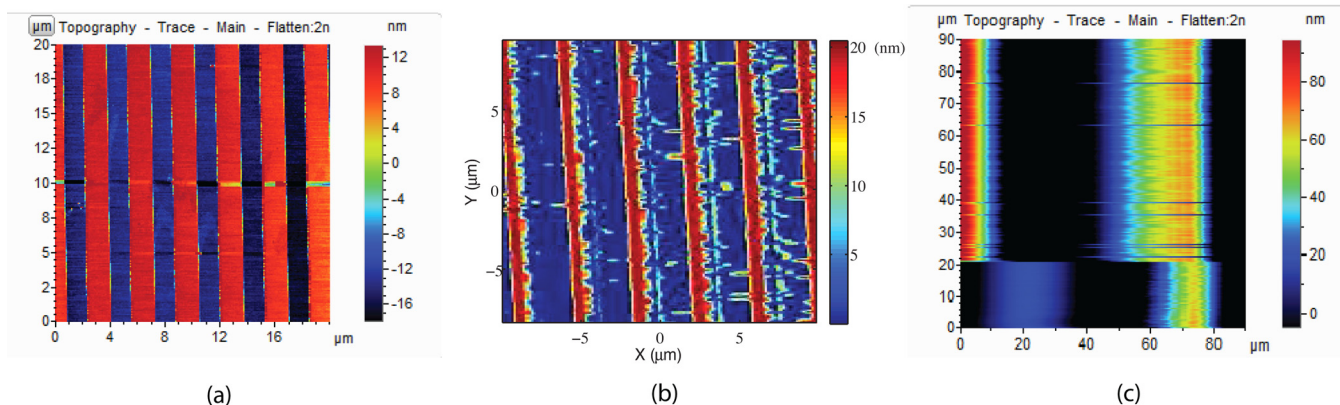


FIG. 1. Imaging of a linear grating. (a) Standard raster scan at 1 line/s, 512 pixel resolution (8.5 min). (b) \hat{w}_2 image and (c) height signal and 24.41 lines/s, 512 pixel resolution. (21 s).

represents the tracking error but with a relatively longer transient process after a change in the sample profile. At both low and moderate speeds, then, the estimate $\hat{w}_2(k)$ behaves similarly to the amplitude signal in tapping mode.

If the AFM is operated well beyond ω_B , then the controller has no time to respond to changes in the sample profile. At such rates, we have that in Eq. (7), $\Gamma_{\omega_B}[r(k) - \mathcal{D}(y(k))] \simeq 0$. As a result, $\hat{w}_2(k) \simeq h(s(k))$, and thus, the signal represents the sample profile. It should be noted, however, that the lack of response of the z -piezos implies that the tip-sample interaction force is no longer finely controlled. This is discussed further in the experimental results below.

To illustrate the performance of the estimator of the sample profile, we applied it on an Agilent 5500 equipped with a MAC III module and operated in its Acoustic AC (AAC) mode (a form of tapping mode). The manufacturer's specifications give the bandwidth of the open-loop piezoelectric actuators in all directions to be in the range of 5 kHz–10 kHz, with closed-loop to be around 1 kHz. In these experiments, an Agilent MAC II Lever probe with a resonance of 75.8 kHz was used. The data acquisition and the implementation of the observer and the calculation of w_2 were done using a compact Reconfigurable Input-Output (cRIO) system (cRIO 9082, National Instruments). This system includes an embedded 1.33 GHz real-time processor and an LX150 FPGA from the Xilinx Spartan-6 family. The cRIO was outfitted with a 1Ms/s high-speed analog-digital

converter (ADC) (NI 9215, National Instruments) for sampling the cantilever position, cantilever drive and the cantilever amplitude (deflection), a 100 Ks/s ADC (NI 9223, National Instruments) for sampling the z -controller output for the height information of the sample and a 100 Ks/s digital-to-analog converter (DAC). The software was written in LABVIEW 12.0 (National Instruments).

In the first experiment, a linear grating (TGZ01, MikroMash) with a feature height of 20 nm and a pitch width of 3.3 μm was imaged. A regular raster scan was performed first with a scan range of 20 μm, a line rate of 1 Hz, and a pixel number of 512. The resulting image, shown in Fig. 1(a), took 8.5 min to acquire. The tip speed was then pushed to the limit of the instrument by setting the line rate to 24.41 Hz and the scan range to 90 μm. To avoid nonlinearities such as sample tilt and bowing due to the large scan range as well as to ensure good tip-sample interaction, only the center 20 μm of data was used. The total scan time was only 21 s. From this data, two images with pixel numbers of 512 were generated, one from the w_2 signal (Fig. 1(b)) and the other from the height signal measured from the instrument (Fig. 1(c)). As expected, at this fast rate and with this large scan range, the z -controller performed quite poorly and the corresponding height image contains little useful information. The w_2 signal clearly shows the main features of the sample.

The second experiment was on lambda DNA. The DNA was diluted in purified water to a concentration of 40 μg/ml.

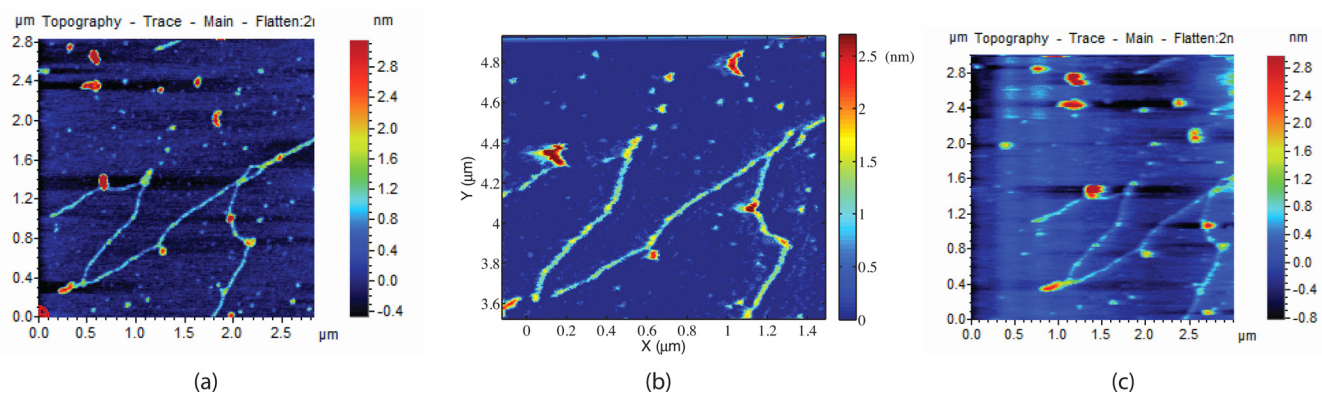


FIG. 2. Imaging of lambda DNA. (a) Standard raster scan at 1 line/s, 512 pixel resolution (8.5 min). (b) \hat{w}_2 image and (c) height signal and 24.41 lines/s, 512 pixel resolution. (21 s).

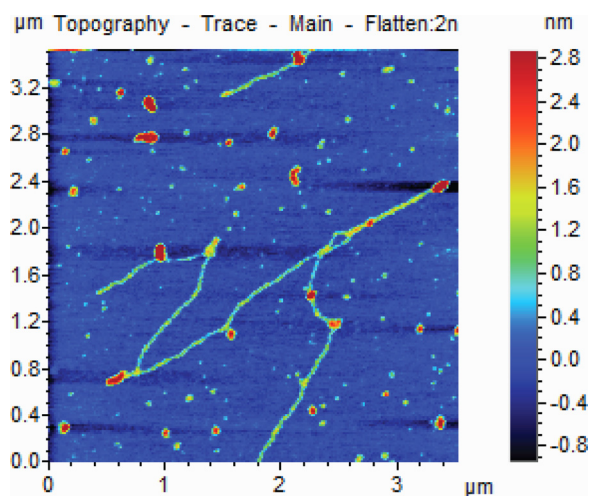


FIG. 3. Raster scan (1 line/s) of the sample in Fig. 2 after high speed imaging, showing no sample damage.

A quantity of $30\ \mu\text{l}$ was deposited on a freshly cleaved mica substrate (9.9 mm, PELCO Mica Discs), incubated for 5 min to allow the DNA to adhere to the substrate and then flushed using a volume of 1 ml purified water to rinse off any unbound samples. It was then dried in air for 24 h.

A standard raster-scan image of the DNA was taken first, with a line rate of 1 Hz, a scan range of $3\ \mu\text{m}$, and a pixel number of 512. The resulting image, acquired in 8.5 min, is shown in Fig. 2(a). The scan rate was then increased to 24.41 Hz in the same fashion as with the linear grating. The \hat{w}_2 and height images are shown in Figs. 2(b) and 2(c), respectively. These images were acquired in 21 s. Since the scan range was smaller than used with the grating, the tip speed was much slower and the height image contains significant information. It is degraded, however, by artifacts such as parachuting, loss of height information, and other dynamic effects that do not show up in the \hat{w}_2 signal.

To calibrate the \hat{w}_2 signal in Fig. 2, the linear grating results were used since they had a known height of 20 nm. This is essentially the same calibration procedure used in standard AFM topography imaging, though no flattening process is needed. The height of the DNA from the \hat{w}_2 image in Fig. 2(b) corresponds well with that of the original raster scan in Fig. 2(a).

The high line rate, relative to the bandwidths of the scanning stage as z -actuation, resulted in vibrations that are clearly apparent in Figs. 2(b) and 2(c). These vibrations, however, did not affect the imaged features of the DNA. We note that vibrations due to the scanning rate also appear in the high-speed scan of the grating in Fig. 1, but it is small relative to the magnitude of the signal. These results illustrate that the limiting element is the lateral scan rate; the use

of advanced stages¹⁴ would allow for line rates on the order of a kHz and the corresponding 50-fold or better increase in frame rate.

As noted above, however, operating the AFM beyond the bandwidth of the z -actuator implies that the tip-sample interaction is no longer controlled. High-speed scanning, therefore, risks applying high vertical forces to the sample. (Since imaging is being performed in tapping mode with cantilever dither frequencies in the tens of kHz to MHz range, shear forces should remain small.) This issue also arises in high-speed contact-mode AFM. Experiments in imaging collagen at frames rates in excess of 1000 frames per second, however, have been performed without damage to the sample.¹⁵

To demonstrate on the DNA sample that repeated imaging is possible at rates beyond the bandwidth of the z -controller, the sample shown in Fig. 2 was imaged using a standard raster scan after the high-speed scan was complete. The resulting image, shown in Fig. 3, shows no evidence of damage from the scanning process.

We thank Professor Josephson and Dr. Cho (Harvard Medical School) for providing the DNA sample and Dr. Sahoo (University of Bristol) for insightful and helpful discussions on our approach. This work was supported in part by the National Institute of General Medical Sciences (8 R21 GM103530-03) from the National Institutes of Health.

- ¹G. Binnig, C. Quate, and C. Gerber, *Phys. Rev. Lett.* **56**, 930 (1986).
- ²D. Y. Abramovitch, S. B. Andersson, L. Y. Pao, and G. Schitter, in *Proceedings American Control Conference* (2007), p. 3488.
- ³N. Kodera, D. Yamamoto, R. Ishikawa, and T. Ando, *Nature* **468**, 72 (2010).
- ⁴G. E. Fantner, G. Schitter, J. H. Kindt, T. Ivanov, K. Ivanova, R. Patel, N. Holten-Andersen, J. Adams, P. J. Thurner, I. W. Rangelow, and P. K. Hansma, *Ultramicroscopy* **106**, 881–887 (2006).
- ⁵G. Schitter and M. J. Rost, *Mater. Today* **11**, 40–48 (2008).
- ⁶T. Ando, *Nanotechnology* **23**, 062001 (2012).
- ⁷P. I. Chang, P. Huang, J. Maeng, and S. B. Andersson, *Rev. Sci. Instrum.* **82**, 063703 (2011).
- ⁸I. A. Mahmood and S. O. R. Moheimani, *Nanotechnology* **20**, 365503 (2009).
- ⁹Y. K. Yong, S. O. R. Moheimani, and I. R. Petersen, *Nanotechnology* **21**, 365503 (2010).
- ¹⁰T. Tuma, J. Lygeros, V. Kartik, A. Sebastian, and A. Pantazi, *Nanotechnology* **23**, 185501 (2012).
- ¹¹D. R. Sahoo, A. Sebastian, and M. V. Salapaka, *Int. J. Robust Nonlinear Control* **15**, 805 (2005).
- ¹²D. R. Sahoo, A. Sebastian, and M. V. Salapaka, *Appl. Phys. Lett.* **83**, 5521 (2003).
- ¹³P. Huang and S. B. Andersson, in *Proceedings IFAC Symposium on Mechatronics* (2013), p. 153.
- ¹⁴Y. K. Yong, S. O. R. Moheimani, B. J. Kenton, and K. K. Leang, *Rev. Sci. Instrum.* **83**, 121101 (2012).
- ¹⁵L. Picco, L. Bozec, A. Ulcinas, D. J. Engledew, M. Antognozzi, M. A. Horton, and M. Miles, *Nanotechnology* **18**, 044030 (2007).